Measurement of the nuclear multiplicity ratio for K_s^0 hadronization at CLAS

A. Daniel[ac], K. Hicks[ac], W.K. Brooks[al,aj], H. Hakobyan[al,ap], K.P. Adhikari[ad], D. Adikaram[ad], M. Aghasyan[s], M. Amarian[ad], M. Anghinolfi[t], H. Avakian[aj], H. Baghdasaryan[an,ad], M. Battaglieri[t], V. Batourine[aj,y], I. Bedlinskiy[w], R. P. Bennett[ad], A.S. Biselli[l,f], C. Bookwalter[n], W.J. Briscoe[p], V.D. Burkert[aj], D.S. Carman[aj], L. Casey[g], A. Celentano[t], S. Chandavar[ac], P.L. Cole[q,g,aj], M. Contalbrigo[r], V. Crede[n], A. D'Angelo[u,ag], N. Dashyan[ap], R. De Vita[t], E. De Sanctis[s], A. Deur[aj], B. Dey[f], R. Dickson[f], C. Djalali[ai], G.E. Dodge[ad], D. Doughty[i,aj], H. Egiyan[aj], L. El Fassi[a], L. Elouadrhiri[aj], P. Eugenio[n], G. Fedotov[ai], S. Fegan[am], M.Y. Gabrielyan[m], N. Gevorgyan[ap], G.P. Gilfoyle[af], K.L. Giovanetti[x], F.X. Girod[aj], J.T. Goetz[c], W. Gohn[j], E. Golovatch[ah], R.W. Gothe[ai], K.A. Griffioen[ao], M. Guidal[v], L. Guo[m,aj], C. Hanretty[an], D. Heddle[i,aj], M. Holtrop[aa], C.E. Hyde[ad], Y. Ilieva[ai,p], D.G. Ireland[am], B.S. Ishkhanov[ah], E.L. Isupov[ah], S.S. Jawalkar[ao], H.S. Jo[v], K. Joo[j], N. Kalantarians[an], D. Keller[ac], M. Khandaker[ab], P. Khetarpal[m], A. Kim[y], W. Kim[y], A. Klein[ad], F.J. Klein[g], V. Kubarovsky[aj,ae], S.V. Kuleshov[al,w], V. Kuznetsov[y], H.Y. Lu[f], I .J .D. MacGregor[am], Y. Mao[ai], N. Markov[j], M. Mayer[ad], J. McAndrew[k], B. McKinnon[am], C.A. Meyer[f], T. Mineeva[j], M. Mirazita[s], V. Mokeev[aj,ah,1], H. Moutarde[h], E. Munevar[p], P. Nadel-Turonski[aj], A. Ni[y], S. Niccolai[v], G. Niculescu[x], I. Niculescu[x], M. Osipenko[t], A.I. Ostrovidov[n], M. Paolone[ai], L. Pappalardo[r], R. Paremuzyan[ap], K. Park[aj,y], S. Park[n], E. Pasyuk[aj,b], S. Anefalos Pereira[s], E. Phelps[ai], S. Pisano[s,ag], O. Pogorelko[w], S. Pozdniakov[w], J.W. Price[d], S. Procureur[h], D. Protopopescu[am], B.A. Raue[m,aj], G. Ricco[o,2], D. Rimal[m], M. Ripani[t], G. Rosner[am], P. Rossi[s], F. Sabatié[h], M.S. Saini[n], C. Salgado[ab], D. Schott[m], R.A. Schumacher[f], H. Seraydaryan[ad], Y.G. Sharabian[aj], G.D. Smith[am], D.I. Sober[g], D. Sokhan[v], S.S. Stepanyan[y], S. Stepanyan[aj], S. Strauch[ai,p], M. Taiuti[o,2], W. Tang[ac], C.E. Taylor[q], S. Tkachenko[ai], M. Ungaro[j,ae], B .Vernarsky[f], M.F. Vineyard[ak], H. Voskanyan[ap], E. Voutier[z], D.P. Watts[k], L.B. Weinstein[ad], D.P. Weygand[aj], M.H. Wood[e,ai], L. Zana[aa],

[1]Current address: Skobeltsyn Nuclear Physics Institute, 119899 Moscow, Russia
[2]Current address: INFN, Sezione di Genova, 16146 Genova, Italy

N. Zachariou[p], B. Zhao[ao], Z.W. Zhao[an]

[a]*Argonne National Laboratory, Argonne, Illinois 60441*
[b]*Arizona State University, Tempe, Arizona 85287-1504*
[c]*University of California at Los Angeles, Los Angeles, California 90095-1547*
[d]*California State University, Dominguez Hills, Carson, CA 90747*
[e]*Canisius College, Buffalo, NY*
[f]*Carnegie Mellon University, Pittsburgh, Pennsylvania 15213*
[g]*Catholic University of America, Washington, D.C. 20064*
[h]*CEA, Centre de Saclay, Irfu/Service de Physique Nucléaire, 91191 Gif-sur-Yvette, France*
[i]*Christopher Newport University, Newport News, Virginia 23606*
[j]*University of Connecticut, Storrs, Connecticut 06269*
[k]*Edinburgh University, Edinburgh EH9 3JZ, United Kingdom*
[l]*Fairfield University, Fairfield CT 06824*
[m]*Florida International University, Miami, Florida 33199*
[n]*Florida State University, Tallahassee, Florida 32306*
[o]*Università di Genova, 16146 Genova, Italy*
[p]*The George Washington University, Washington, DC 20052*
[q]*Idaho State University, Pocatello, Idaho 83209*
[r]*INFN, Sezione di Ferrara, 44100 Ferrara, Italy*
[s]*INFN, Laboratori Nazionali di Frascati, 00044 Frascati, Italy*
[t]*INFN, Sezione di Genova, 16146 Genova, Italy*
[u]*INFN, Sezione di Roma Tor Vergata, 00133 Rome, Italy*
[v]*Institut de Physique Nucléaire ORSAY, Orsay, France*
[w]*Institute of Theoretical and Experimental Physics, Moscow, 117259, Russia*
[x]*James Madison University, Harrisonburg, Virginia 22807*
[y]*Kyungpook National University, Daegu 702-701, Republic of Korea*
[z]*LPSC, Universite Joseph Fourier, CNRS/IN2P3, INPG, Grenoble, France*
[aa]*University of New Hampshire, Durham, New Hampshire 03824-3568*
[ab]*Norfolk State University, Norfolk, Virginia 23504*
[ac]*Ohio University, Athens, Ohio 45701*
[ad]*Old Dominion University, Norfolk, Virginia 23529*
[ae]*Rensselaer Polytechnic Institute, Troy, New York 12180-3590*
[af]*University of Richmond, Richmond, Virginia 23173*
[ag]*Universita' di Roma Tor Vergata, 00133 Rome Italy*
[ah]*Skobeltsyn Nuclear Physics Institute, Skobeltsyn Nuclear Physics Institute, 119899 Moscow, Russia*
[ai]*University of South Carolina, Columbia, South Carolina 29208*
[aj]*Thomas Jefferson National Accelerator Facility, Newport News, Virginia 23606*
[ak]*Union College, Schenectady, NY 12308*
[al]*Universidad Técnica Federico Santa María, Casilla 110-V Valparaíso, Chile*
[am]*University of Glasgow, Glasgow G12 8QQ, United Kingdom*
[an]*University of Virginia, Charlottesville, Virginia 22901*
[ao]*College of William and Mary, Williamsburg, Virginia 23187-8795*

2

^{ap}*Yerevan Physics Institute, 375036 Yerevan, Armenia*

Abstract

The influence of cold nuclear matter on lepto-production of hadrons in semi-inclusive deep inelastic scattering is measured using the CLAS detector in Hall B at Jefferson Lab and a 5.014 GeV electron beam. We report the K_s^0 multiplicity ratios for targets of C, Fe, and Pb relative to deuterium as a function of the fractional virtual photon energy z transferred to the K_s^0 and the transverse momentum squared p_T^2 of the K_s^0. We find that the multiplicity ratios for K_s^0 are reduced in the nuclear medium at high z and low p_T^2, with a trend for the K_s^0 transverse momentum to be broadened in the nucleus for large p_T^2.

Keywords: Hadronization, Hadron production, Deep inelastic scattering, Nuclei, Quarks

Hadronization is the process through which partons, created in an elementary reaction, turn into hadrons. An example for this process is lepto-production of hadrons in semi-inclusive deep-inelastic electron-nucleon scattering, where a parton is struck by a virtual photon; as the parton propagates away from the interaction point it picks up partner quarks (antiquarks) to form a hadron. The process of hadronization is changed by the nuclear medium. Nuclear modification of hadron production in deep-inelastic scattering (DIS) was first observed at SLAC [1] followed by EMC [2], E665 [3] and more recently at HERMES [4–6]. The goal of these investigations is to study the mechanism of quark deconfinement followed by propagation and then reconfinement into a hadron, and in particular how the presence of cold nuclear matter affects the hadronization process. Although some rescattering of the quark/hadron in nuclear matter is expected, calculations [7, 8] for the HERMES data suggest that the effects are more than just simple rescattering–the hadronization mechanism itself is changed due to the propagation through nuclear matter. In addition to understanding the fundamental features of hadronization, a detailed understanding of the nuclear modifications is important for the interpretation of ultra-relativistic heavy ion collisions, as well as the study of neutrino oscillations using nuclear targets in the GeV energy

range. A recent review on the subject of hadronization and parton propagation can be found in reference [9].

The observables reported in the present paper are the multiplicity ratios as a function of $z = E_h/\nu$, the fraction of the virtual-photon energy carried by the hadron in the target rest frame, and its transverse momentum squared, p_T^2. The transverse momentum is defined as the perpendicular component of the hadron's momentum measured with respect to the direction of momentum transfer in electron scattering. The multiplicity ratio R_A^h is defined as the ratio of the number of hadrons detected, normalized to the number of electrons measured in the DIS kinematics for a nuclear target with mass number A, divided by the same quantities for a deuterium target(D);

$$R_A^h = \frac{\left[N_h \left(z, p_T^2, Q^2, \nu \right) / N_{e^-}^{DIS} \left(\nu, Q^2 \right) \right]_A}{\left[N_h \left(z, p_T^2, Q^2, \nu \right) / N_{e^-}^{DIS} \left(\nu, Q^2 \right) \right]_D}, \tag{1}$$

where N_h is the number of hadrons and $N_{e^-}^{DIS}$ is the number of scattered electrons detected in the specified kinematic bins. Here, Q^2 is the negative of the four-momentum of the virtual photon squared and ν is the energy of the virtual photon. For most of the explored kinematic range R_A^h shows a reduction from unity, although at low z and high p_T^2 it shows an enhancement. Hadron *formation lengths*, the characteristic distances over which hadrons form, can be extracted from R_A^h [10].

In certain theoretical models, the transverse momentum is broadened for hadronization from nuclear targets as compared with the distribution measured from deuterium, and the amount of broadening is sensitive to gluonic radiation by the quark before it evolves into a hadron [9, 11, 12]. By varying the nuclear radius, measurements of the broadening as a function of the kinematic variables allow one to infer the length scale (known as the *production length*) over which the quark is deconfined.

Since hadronization is a nonperturbative QCD process that as yet cannot be calculated from first principles, one must rely on models to interpret the observed nuclear dependence of hadronization. In particular, several hadron species are required to analyze the flavor dependence of the observables, to unravel the reaction mechanisms involved and to give insight into the fundamental principles governing hadron formation. Of special interest is the hadronization into strange mesons as compared with non-strange mesons. In the HERMES data [6], the z dependence of R_A^h in the medium for π^+, π^- and π^0 is nearly identical for a given nucleus. However, R_A^h for K^+ is

systematically larger than for K^-. The difference for the charged kaons can be explained due to the larger nuclear absorption for K^- compared to K^+. Also, note that pions have only non-strange valence quarks, K^+ has a non-strange valence quark while K^- has a non-strange antiquark and strange quark content. Thus, the production of a negative kaon requires further complicated string breaking mechanisms and fewer leading hadrons are expected to be K^- as compared to K^+.

While the HERMES measurements for the hadronization effects in π^0 production looked very similar to $\pi^\pm$, they did not report any K^0 hadronization results. Strangeness production can give a unique insight into the hadronization process, since the strange quark is likely to come directly from the "string-breaking" process [6]. Different hadron species, such as the K_s^0, are relevant to the study of the flavor dependence of hadronization and the mass dependence of quark energy loss. In this letter, we report for the first time on K_s^0 hadronization measured using the CLAS detector at Jefferson Lab. Our results show, like the HERMES results, that the hadronization mechanism is affected by the presence of the nuclear medium. Of course, the K_s^0 is a mixture of K^0 and $\bar{K}^0$, but just as K^+ hadronization dominates over K^- (presumably due to the non-strange valence quark in the K^+) we expect that most of the K_s^0 signal is dominated by K^0 hadronization, with a smaller contribution from $\bar{K}^0$.

The experiment was carried out using the CLAS detector [13] at the Thomas Jefferson National Accelerator Facility. The data presented here are from the E02-104 [14] experiment. An electron beam of 5.014 GeV was incident on targets of liquid deuterium, solid carbon, iron and lead. The targets were arranged in a mechanical structure that allowed one solid nuclear target to be in the beam at the same time as (and slightly downstream of) the liquid deuterium target [15]. The length of liquid target was about 2 cm and the separation distance between solid and liquid targets was approximately 4 cm. This allowed for reduced systematic uncertainties in the ratios of hadrons measured by the CLAS detector. The scattered electron and the produced hadrons were detected in coincidence by the CLAS detector. Details of the experiment are described in Ref. [16].

The DIS kinematics covered by the present experiment are shown in Fig. 1, where Q^2 is plotted versus ν and also versus Bjorken $x = Q^2/(2M\nu)$, where M the nucleon mass. Constraints have been applied, limiting the kinematic variables to $Q^2 > 1.0$ GeV^2, $W^2 > 4.0$ GeV^2 and $y < 0.85$, where W^2 is the squared invariant mass of the photon-nucleon system, $y = \nu/E$
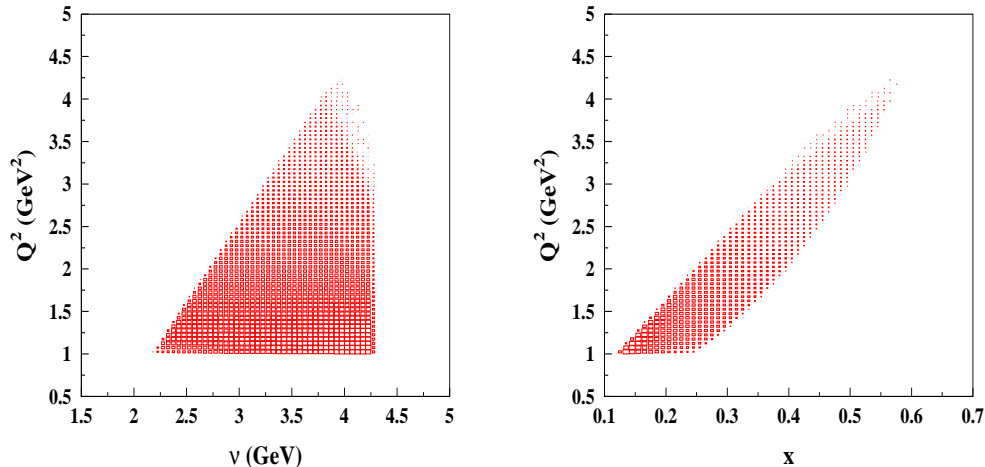
5

Figure 1: Distribution of Q^2 versus ν (left) and x (right), for DIS events from a 5.014 GeV electron beam on a liquid deuterium target, after the kinematic cuts described in the text.

the energy fraction of the virtual photon in the target rest frame, and E is the beam energy. The constraint on y is applied to reduce the magnitude of radiative corrections. The range in x depends on Q^2 and extends from $x = 0.1$ at the lowest Q^2 up to $x = 0.55$ at the highest Q^2. Though the sea quarks may have non-negligible contribution at the smallest x values probed in this experiment, for x greater than about 0.3 the virtual photon is likely to strike a valence quark. Note that the kinematics of the CLAS results are different from those of HERMES results, which had higher ν and hence lower x, extending down to 0.023.

The K_s^0's were found from fits to the invariant mass distribution of $\pi^+\pi^-$ pairs produced. After identifying the scattered electron, K_s^0 invariant mass spectra $M(\pi^+, \pi^-)$ is formed from the combination of all charged pion pairs, detected in CLAS. For a given bin in z, and integrated over all electron kinematics and all other hadron variables, a clear peak in $M(\pi^+, \pi^-)$ is seen at the mass of the K_s^0 as shown in the top plots of Fig. 2 for both the liquid deuterium (left) and solid Pb (right) targets. Similarly, plots showing the K_s^0 peaks for a bin in p_T^2 after integrated over all electron kinematics and all other hadron variables are shown in the bottom plots of Fig. 2. Although substantial, the background from uncorrelated $\pi^+\pi^-$ pairs is smooth and is easily fit by a polynomial. The K_s^0 peak was fit using an unconstrained
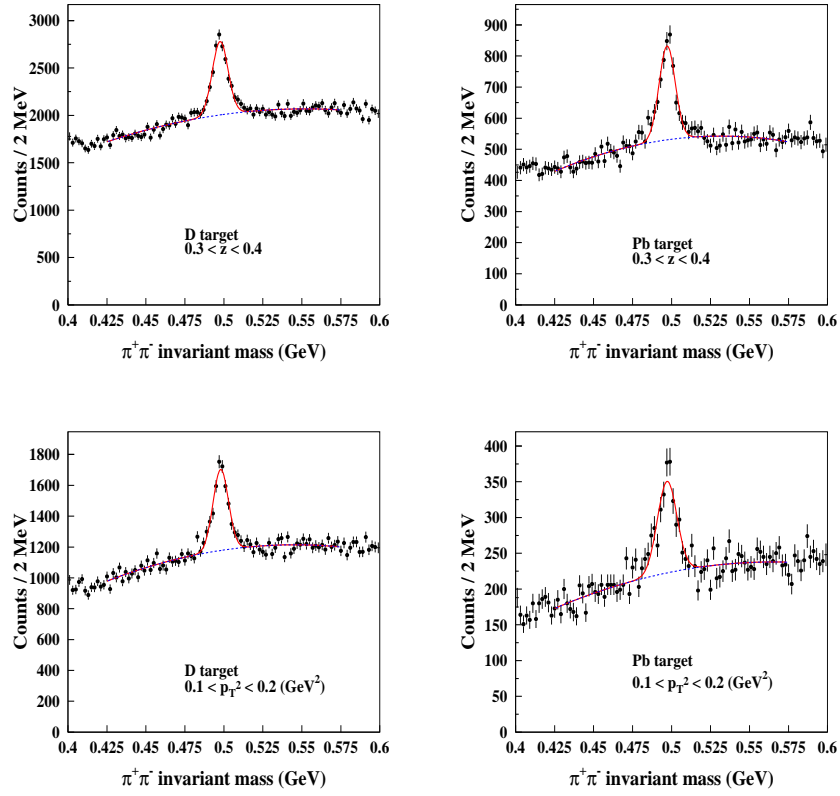
Figure 2: Invariant mass of two oppositely charged pions, showing a peak at the K^0 mass, for the liquid deuterium target (left) and the solid Pb target (right) for selected kinematic bins: $0.3 < z < 0.4$ (top) and $0.1 < p_T^2 < 0.2$ GeV^2 (bottom). The x-bin size is 2 MeV.

Gaussian. The statistical uncertainties are determined directly from the fit parameters.

Results for R_A^h as a function of z and of p_T^2 for K_s^0 hadronization are shown in Figs. 3 and 4, respectively, for the carbon, iron and lead targets. The kinematic dependence on a given variable is extracted while integrating over all other variables within the acceptance of the experiment. Results for R_A^h vs. z for the charged kaons from the HERMES experiment are also shown in left panel of Fig. 3. For comparison, we have plotted only the results for the xenon target from the HERMES experiment; results for several nuclei and different hadrons are available in Ref. [6]. For the p_T^2 dependence studies, the data presented are limited to $0.3 < z < 0.8$ to reduce the possible contamination from target fragmentation and from exclusive channels. The ratios of K_s^0 have been normalized by the number of DIS electrons for each target and corrected for geometrical detector acceptance for each target as calculated by Monte Carlo simulations using a PYTHIA event generator [16, 17]. The acceptance correction was applied on a bin-by-bin basis. No corrections have been applied to the data for QED radiative effects, which were too small to measure with the present statistics. However, our studies showed that these corrections are less than 5% for the multiplicity ratios and this is included in the systematic uncertainty.

Several sources contribute to the overall systematic uncertainty in the multiplicity ratios. Details of the systematic uncertainty studies are described in Ref. [18]. The systematic uncertainty in the acceptance correction was found to be less than 5% for the z dependence (except for the lowest z bin where this uncertainty is estimated to be 16%) and less than 8% for the p_T^2 dependence. The systematic uncertainty associated with particle identification for the multiplicity ratios was found to be less than 3%. To account for the possible systematic uncertainty in the fitting procedures we have assigned a 4% uncertainty in R_A^h vs. z results and a 5% uncertainty in R_A^h vs. p_T^2. The total uncertainty is obtained by adding systematic and statistical uncertainties in quadrature, and are shown by the longer error bars in Figs. 3 and 4.

Fig. 3 shows that, for $z > 0.3$, fewer K_s^0 are seen from nuclear targets (normalized by the number of DIS events) than from deuterium while at $z < 0.3$ the ratio shows a trend to be bigger than unity. At lower z, effects such as nuclear rescattering, including (π, K) reactions, and target fragmentation are likely to contribute to the number of K_s^0 measured. The same effect at low z for K^+ hadronization has already been noted by HERMES [5]. The
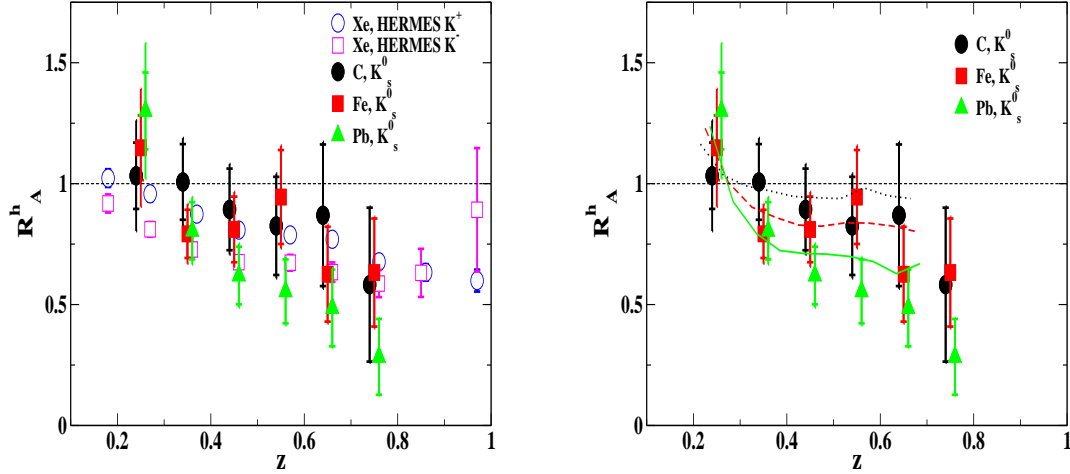
Figure 3: Left panel shows the CLAS data from the EG2 experiment for the hadronic multiplicity ratio for K_s^0 versus z along with HERMES results [6] for charged kaons for the Xe nuclei. Right panel shows the CLAS results along with the results derived from calculations of Ref. [7] for Pb (solid line), Fe (dashed line) and C (dotted line). Data points are shown with different symbols as given in the legend. The inner error bars represent the statistical uncertainty, while the outer ones show the total uncertainty. For clarity, the HERMES points are shifted by +0.02 units in z and the C and Pb points are shifted by -0.01 and +0.01 units in z, respectively.

trend of the CLAS K_s^0 hadronization data is similar to that of the HERMES results, where more attenuation is seen as z increases, with larger attenuation factors for the heaviest target. The present uncertainties are large due to the limited statistics, however the data agree reasonably well with predictions [7] as shown in right panel of Fig. 3.

The theoretical calculations shown in Fig. 3 and presented in Ref. [7] are carried out in the framework of a probabilistic coupled-channel transport model based on the Boltzmann-Uehling-Uhlenbeck equation, which allows for detailed treatment of the final-state interactions beyond simple absorption mechanisms. It starts with the Lund string fragmentation picture as embodied by PYTHIA [17] and extracts two points for each event: (i) the location in space where the struck quark breaks the string, and (ii) the location where the quark joins with an antiquark to form a meson. This is done event-by-event, in the context of a Monte Carlo calculation. Medium effects

9

are included by assuming a phenomenological transition from a pre-hadronic scattering cross section to a full cross section constrained by hadronic beam data. A function linear in the formation and production times is found to best fit the HERMES and EMC data (see Equation 3 and Fig. 1 of Ref. [7]). Note that the calculations presented in [7] are for K^0 and $\bar{K}^0$. For a given nucleus, we show the average of the above calculations to compare with the K_s^0 data.

In some theoretical models [9], the decrease in R_A^h with z can be explained by the struck parton losing energy before picking up a partner antiquark, on the way to forming a hadron. One mechanism of energy loss is gluon radiation in the nuclear medium, although other mechanisms such as absorption [19] are also possible. This energy loss reduces the hadron energy E_h and hence reduces z for hadronization from a nucleus. Because the fragmentation functions have a steep dependence on z, the ratio R_A^h generates a steady decrease with z. Other models [9] assume a decreased formation length for the struck quark to pick up a partner antiquark, followed by rescattering and absorption of the resulting hadron.

The results for K_s^0 at CLAS kinematics show R_A^h for $z > 0.6$ with the Pb target to be below the HERMES results for charged kaons from xenon. One must be careful when comparing these two data sets because of the different kinematic ranges; however, the CLAS kinematics provide an additional point of constraint for theoretical models of hadronization. Note that neutral kaons have a smaller reaction cross section than pions, and hence rescattering effects are minimized for K^0 hadronization. In particular, the K^0 data should be less affected by hadronic final-state interactions than pions, and more sensitive to QCD effects (such as gluon radiation) as the quark propagates through cold nuclear matter.

Fig. 4 shows the multiplicity ratios as a function of the transverse momentum squared. At high p_T^2, there are very few K_s^0 events, leading to large statistical uncertainties. However, at small p_T^2 the statistics are reasonable and there is a clear target-dependence to the nuclear attenuation for $p_T^2 < 0.1$ GeV^2. The K_s^0 multiplicity ratios then increase as p_T^2 increases and exceed unity at around p_T^2=0.45 GeV^2. This crossover is at lower p_T^2 than for the HERMES results. Furthermore, the CLAS data have a steeper slope with p_T^2 than those measured by HERMES. Both CLAS and HERMES data show that R_A^h levels off for lighter targets at low p_T^2, yet continues to decrease for heavier targets at low p_T^2.

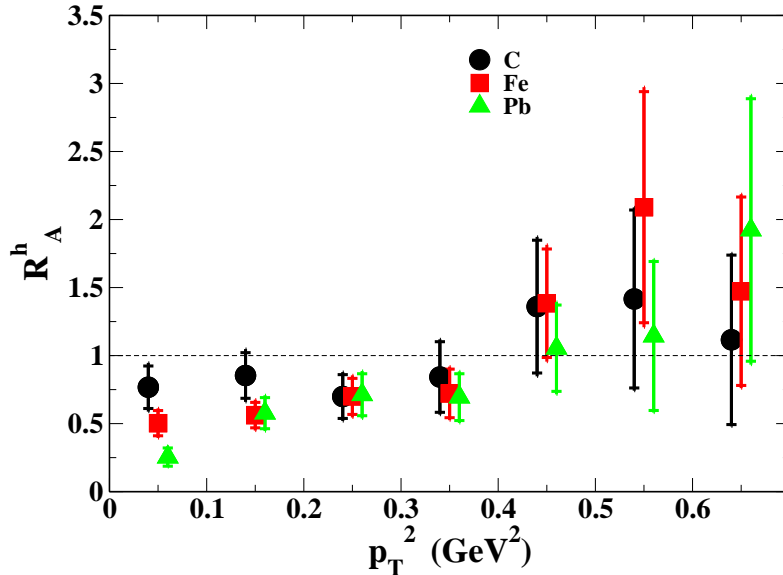The increase in R_A^h with p_T^2 was seen previously by EMC [2] and HER-

Figure 4: CLAS data for the hadronic multiplicity ratio for K_s^0 as a function of p_T^2 for $0.3 < z < 0.8$. Error bars are as in Fig. 3. For clarity, the C and Pb points are shifted by -0.01 and +0.01 units in p_T^2, respectively.

MES [5, 6]. This is known as the Cronin effect [20], in which rescattering of either the parton or the hadron, as well as hadronic final state interactions, pushes events up to larger p_T^2. These effects occur preferentially in nuclear targets. The HERMES data for pions [6, 12] shows that the Cronin effect diminishes for high-z events, which is consistent with predictions from parton rescattering [8]. The question whether this also happens for K_s^0 hadronization must await better statistics, which will be available after the CLAS detector is upgraded in a few years for 12 GeV beam energies.

In summary, we have extracted for the first time the multiplicity ratios for K_s^0 using semi-inclusive deep inelastic scattering with detection of the K_s^0 using the CLAS detector with a 5.014 GeV electron beam incident on both deuterium and nuclear targets. Many systematic effects cancel in the ratio R_A^h, in part because both deuterium and nuclear targets were exposed to beam simultaneously and were separated by only a few centimeters at the

center of CLAS. The z and p_T^2 dependencies of R_A^h follow the trends seen in previous data by HERMES Collaboration at higher ν and Q^2, suggesting that the general mechanism of hadron formation are similar at CLAS kinematics.

In order to fully understand the fundamental principles of the hadron formation as well as the flavor dependence of the observables, a wide spectrum of both baryons and mesons are required. Some of these channels, including more precise pion data, are currently under investigation by the CLAS collaboration. Ultimately, the interpretation of these data will require further theoretical development.

References

[1] L. S. Osborne, et al., Phys. Rev. Lett. 40 (1978) 1624.

[2] J. Ashman, et al., Z. Phys. C52 (1991) 1.

[3] M. R. Adams, et al., Phys. Rev. D 50 (1994) 1836.

[4] A. Airapetian, et al., Eur. Phys. J. C 20 (2001) 479.

[5] A. Airapetian, et al., Phys. Lett. B 577 (2003) 37.

[6] A. Airapetian, et al., Nucl. Phys. B 780 (2007) 1.

[7] K. Gallmeister and U. Mosel, Nucl. Phys. A 801 (2008) 68.

[8] B. Kopeliovich, et al., Nucl. Phys. A 740 (2004) 211.

[9] A. Accardi, F. Arleo, W. K. Brooks, D. D'Enterria, V. Muccifora, Riv. Nuovo Cim. 032 (2010) 439.

[10] A. Bialas and T. Chmaj, Phys. Lett. B 133 (1983) 241.

[11] R. Baier, D. Schiff, B. G. Zakharov, Ann. Rev. Nucl. Part. Sci. 50 (2000) 37.

[12] A. Airapetian, et al., Phys. Lett. B 684 (2010) 114.

[13] B. A. Mecking, et al., Nucl. Instrum. Meth. A 503 (2003) 513.

[14] W. Brooks, et al., Jefferson Lab experiment E02-104. (http://www.jlab.org/exp_prog/CEBAF_EXP/index.html)

[15] H. Hakobyan, et al., Nucl. Instr. Meth. A 592 (2008) 218.

[16] H. Hakobyan, Ph.D. thesis, Yerevan State University (http://www.jlab.org/Hall-B/general/clas_thesis.html) (2007).

[17] T. Sjostrand, et al., Computer Physics Commun. 135 (2001) 238.

[18] A. Daniel and K. Hicks, CLAS analysis Note, Report no. 2011-102, (2011).

[19] A. Accardi, D. Grunewald, V. Muccifora, H. J. Pirner, Nucl. Phys. A 761 (2005) 67.

[20] J. W. Cronin, et al., Phys. Rev. D 11 (1975) 3105.